Exciton-Charge Annihilation in Organic Semiconductor Films

Justin M. Hodgkiss, Sebastian Albert-Seifried, Akshay Rao, Alex J. Barker, Andrew R. Campbell, R. Alex Marsh, and Richard H. Friend**

This manuscript is dedicated to the memory of Professor Alan G. MacDiarmid

Time-resolved optical spectroscopy is used to investigate exciton-charge annihilation reactions in blended films of organic semiconductors. In donor–acceptor blends where charges are photogenerated via excitons, pulsed optical excitation can deliver a sufficient density of temporally overlapping excitons and charges for them to interact. Transient absorption spectroscopy measurements demonstrate clear signatures of exciton-charge annihilation reactions at excitation densities of $\approx 10^{18}$ cm^{-3}. The strength of exciton-charge annihilation is consistent with a resonant energy transfer mechanism between fluorescent excitons and resonantly absorbing charges, which is shown to generally be strong in organic semiconductors. The extent of exciton-charge annihilation is very sensitive not only to fluence but also to blend morphology, becoming notably strong in donor–acceptor blends with nanomorphologies optimized for photovoltaic operation. The results highlight both the value of transient optical spectroscopy to interrogate exciton-charge annihilation reactions and the need to recognize and account for annihilation reactions in other transient optical investigations of organic semiconductors.

1. Introduction

Bimolecular interactions between excitations in organic semiconductors have received considerable attention because of their impact on the performance of thin-film optoelectronic devices. In organic photovoltaic (OPV) cells, bimolecular charge recombination reduces the extractable photocurrent and photovoltage.[1,2] Excitons are also subject to bimolecular reactions with other excitons and with charges. For example, annihilation reactions between pairs of triplet excitons have been exploited for light upconversion devices,[3] while triplet excitons have been shown to be bimolecularly quenched by charges in films where both are present.[4,5]

The relatively short lifetimes and short diffusion lengths of singlet excitons are often presumed to limit the likelihood of them participating in bimolecular interactions and result in critical excitation densities much higher than operational densities in most devices. However, strongly emissive singlet excitons can radiatively couple over considerably longer lengthscales than other types of excitations that move via short-range electron tunneling steps.[6,7] This provides the possibility of long range resonant energy transfer (RET) between an exciton (donor) and charge (acceptor), as illustrated in **Scheme 1**. The result of RET in this case is exciton quenching and an excited polaron state that can rapidly lose the excess energy via vibrational relaxation.[8–11] Moreover, optical resonance between excitons and charges is generally very strong (even stronger than for exciton–exciton interactions) due to the lattice relaxation effects that red-shift both exciton emission and polaron absorption relative to the neutral ground-state absorption spectrum of π-conjugated semiconductors. Strong optical resonance between excitons and charges has the effect of substantially reducing the density threshold for exciton-charge annihilation (ECA) and therefore making it an important consideration in many situations encountered in devices or time-resolved measurements.

Examples of devices that can operate with sufficiently high excitation densities to be susceptible to ECA include organic lasers,[8] light-emitting transistors,[12] and OPV devices under concentrated solar illumination. This article focuses on another relatively unexplored consequence of ECA—its complicating effect on the measurement and interpretation of transient excitation dynamics in organic semiconductors. Time-resolved optical spectroscopy techniques such as transient absorption (TA) spectroscopy offer unparalleled insight into the dynamics of transient excitations in organic semiconductor devices.[2,5,6,10,13–21] However, by

Dr. J. M. Hodgkiss, Dr. S. Albert-Seifried, A. Rao, Dr. A. R. Campbell, Dr. R. A. Marsh, Prof. R. H. Friend
Cavendish Laboratory, Department of Physics
University of Cambridge, Cambridge, CB3 0HE, UK
E-mail: Justin.Hodgkiss@vuw.ac.nz; rhf10@cam.ac.uk
Dr. J. M. Hodgkiss, A. J. Barker
MacDiarmid Institute for Advanced Materials and Nanotechnology
School of Chemical and Physical Sciences
Victoria University of Wellington
Wellington, PO Box 600, New Zealand

DOI: 10.1002/adfm.201102433

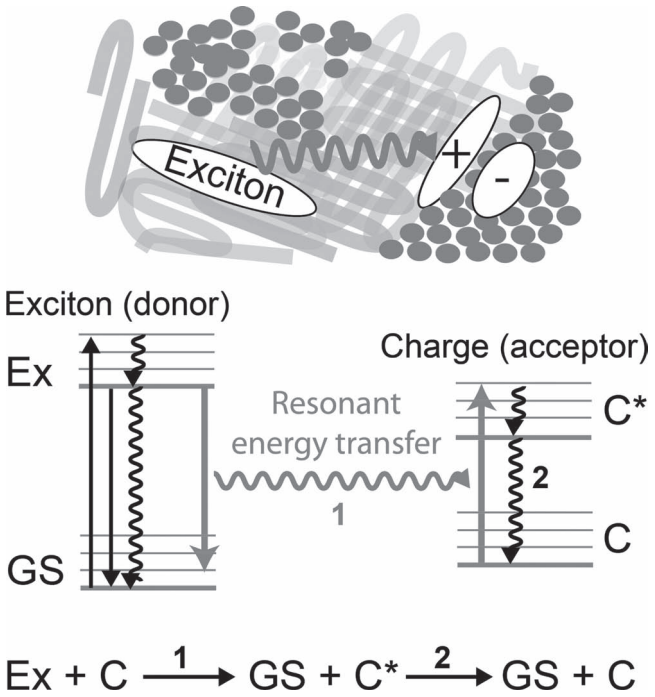

$$Ex + C \xrightarrow{1} GS + C^* \xrightarrow{2} GS + C$$

Scheme 1. ECA via resonant energy transfer between an exciton (Ex) and a charge (C), both of which have stabilized energies relative to the optical gap of the neutral material. Resonant energy transfer (labeled step 1) returns the exciton donor to the groundstate (GS) and leaves a photoexcited charge (C*), which then rapidly loses its excess energy non-radiatively (step 2). This situation can be encountered in a donor–acceptor blend of organic semiconductors (e.g., polymer/fullerene) under pulsed excitation where both excitons and charges coexist at sufficient density to interact.

virtue of delivering light in short pulses, initial excitation densities can be sufficiently high to induce bimolecular interactions.[2,5,6,10,11,16,17] Moreover, in systems that feature a cascade of photophysical processes (e.g., charge generation from excitons), pulsed excitation can lead to substantially different distributions of coexisting excitations than are produced under steady-state conditions. The type and extent of bimolecular interactions therefore depends strongly on the excitation pulsewidth relative to the formation and decay dynamics of transient excitations.

Here, we use TA spectroscopy both as a means of generating coexisting populations of singlet excitons and charges, and as a time-resolved probe of their interaction dynamics. This situation is particularly relevant to time-resolved spectroscopy of charge photogeneration in donor–acceptor blends of OPVs. We start by outlining evidence for ECA in donor-acceptor blends. We then explore the RET mechanism and its generality in organic semiconductor systems. The kinetics of ECA versus competing photoreactions leads to pronounced dependence on blend morphology and excitation intensity, which we discuss along with the resulting effect on photocurrent extraction under pulsed excitation. Our findings highlight the importance of ECA in time-resolved measurements of excitations in organic semiconductors and introduce ways to identify and mitigate its effects.

2. Results and Discussion

2.1. Spectroscopic Evidence for Exciton-Charge Annihilation in Donor–Acceptor Blends Under Pulsed Optical Excitation

Charge generation from singlet excitons in electron donor–acceptor blends is generally found to occur on timescales ranging from femtoseconds to tens of picoseconds and is strongly morphology dependent.[2,16,18,22] Even in a relatively ordered bulk heterojunction blend, the distribution of distances that excitons must diffuse to reach a heterojunction will result in a wide distribution of exciton lifetimes. Given that charge lifetimes (picoseconds to microseconds) are generally longer than exciton lifetimes,[1,2,11,17] optical excitation with pulses shorter than charge lifetimes will result in temporally overlapping populations of excitons and charges. That is to say, under pulsed excitation excitons are present on a timescale over which charges are forming but have not yet recombined.

In this section, we expand on the evidence for ECA that we identified as an artifact in a previous publication about charge generation and recombination in a polymer blend comprised of the electron donor P3HT (poly(3-hexylthiophene) and the electron accepting copolymer F8TBT (poly((9,9-dioctylfluorene)-2,7-diyl-alt-[4,7-bis(3-hexylthien-5-yl)-2,1,3-benzo-thiadiazole]-2,2-diyl)).[11] This blend highlights how to identify ECA because spectroscopic signatures of excitons and charges are easily assigned and ground-state bleach (GSB) signals can be simultaneously probed to quantify the total population of all excitations and their evolution over the interaction timescale of excitons and charges.

Figure 1a shows TA spectra of excitons in P3HT and F8TBT obtained immediately after photoexcitation of thin films of the individual polymers. In both cases, there is a positive differential transmission feature attributed to a GSB at wavelengths corresponding to the polymers absorption. In the case of P3HT, vibronic peaks at 560 nm (0–1) and 610 nm (0–0) are clearly discerned. Both spectra also feature a second positive differential transmission feature at lower energy that coincides with photoluminescence and must therefore be attributed to excitonic stimulated emission (SE). Within the probe wavelength window, the F8TBT spectrum also exhibits a negative differential absorption feature from excitonic photoinduced absorption (PIA) at even lower energy (≈770 nm), while a corresponding feature for P3HT is known to exist outside of our probe window at ≈925 nm.[23] Although both polymers are known to exhibit direct generation of a small population of polaron pairs,[11,18,24] and spectral artifacts have been shown to appear at later times due to temperature modulation effects,[23] we conclude that the TA spectra presented for individual polymers immediately after excitation largely represent excitons.

The TA spectra of the constituent polymers enable us to interpret that of the thermally annealed blend also shown in Figure 1a. The blend TA spectrum exhibits a PIA signal at wavelengths beyond 640 nm, even within 200 fs of photoexcitation. Since the prompt appearance of a PIA signal in this wavelength range cannot be explained by excitations in either of the individual polymers, we attribute it to charge pairs comprised of electrons occupying F8TBT and holes on the P3HT side of

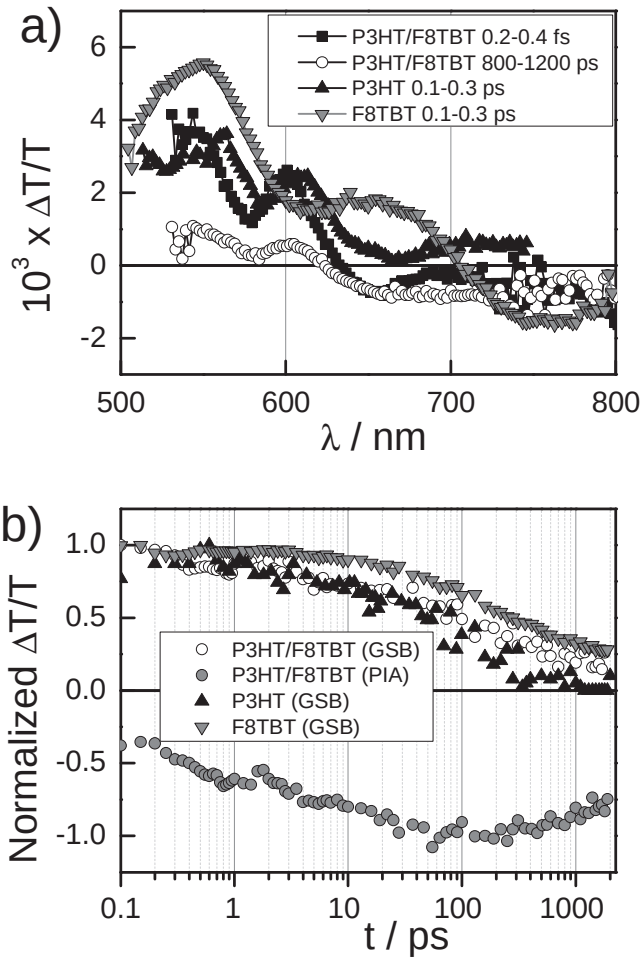

Figure 1. a) TA spectra of P3HT, F8TBT and a thermally annealed blend of the two polymers following 60 fs, 500 nm pulsed excitation (40 μJ cm^{-2}, 10^{14} photons cm^{-2}) at pump–probe delay time ranges indicated on the plot. The P3HT and F8TBT spectra are scaled by a factor of 0.5 for better comparison. b) Normalized TA kinetics for the same films in the GSB region (530–570 nm) and for the blend in the PIA region (650–700 nm).

the interface. The PIA signal broadens to the lower energy side on a timescale of tens of picoseconds, which is consistent with a combination of prompt and delayed charge generation. Initially, a broad PIA feature from promptly formed charge pairs is superimposed with SE from remaining P3HT excitons, which cancels much of the PIA around 700 nm. The underlying broad PIA feature is revealed beyond 100 ps when the remaining excitons have diffused to charge-separating interfaces and no SE remains.

Charge generation kinetics are resolved via the time-evolution of the 650–700 nm PIA feature in Figure 1b. The PIA signal appears within the first 100 fs and grows with a characteristic timescale of a few picoseconds before reaching a maximal value at approximately 100 ps. The subsequent PIA decay by approximately 30% within 2 ns indicates that a significant proportion of photogenerated charge-pairs recombine on a sub-nanosecond timescale, the implications of which we have discussed elsewhere.[11] The timescale of charge generation in the blend can be compared with that of inherent exciton decay measured for the individual polymers under the same conditions to assess the yield of charge generation. The GSB kinetics of the constituent polymers shown in Figure 1b show that the time taken for half of the excitations to return to the ground state is ≈300 ps for F8TBT and ≈100 ps for P3HT, which constitutes the lowest energy exciton state in the blend. Exciton decay may be accelerated by some degree of exciton-exciton annihilation (EEA) at the fluence used here. However, it is clear that the timescale of charge generation in the blend is still substantially faster than inherent exciton lifetimes measured under the same conditions. This timescale disparity is expected to result in near unit charge generation efficiencies, consistent with the strong photoluminescence quenching observed for the same blend under steady state photoexcitation.[22]

This simple picture is challenged by considering the GSB recovery kinetics for the blend (also shown in Figure 1b). The GSB signal of the blend decays on a similar timescale as for unblended P3HT for approximately the first 100 ps. Since the GSB signal at $\lambda < 640$ nm applies to both charged and neutral excitations, its magnitude quantitatively reflects the total population of excitations, assuming that all excitations have the same bleaching cross-section and neglecting the weak effect of temperature modulation artifacts on this timescale.[23] Fast and efficient charge generation followed by charge recombination on a slower timescale (beyond 100 ps) should therefore result in conservation of the GSB signal until the onset of charge recombination. The GSB decay within the first 100 ps cannot be explained by slow and non-competitive charge generation kinetics because that situation would not explain the rapid appearance of the charge-based PIA, efficient PL quenching, and reasonable yields of extracted photocurrent in devices under weak steady state illumination. Nor can the GSB decay be explained by rapid charge recombination (either monomolecular or bimolecular) since that would not produce the observed buildup of charges peaking at ≈100 ps. Given that the GSB decay for the blend within the first ≈100 ps is faster than for neat F8TBT and similar to that of neat P3HT in spite of a significant GSB contribution from charges in the blend, we must conclude that the decay of excitons to the ground-state is accelerated in the blend under pulsed excitation. Although a density-dependent decay channel such as EEA may operate in the neat P3HT film under the same excitation intensity, we emphasize that exciton decay to the ground state is accelerated even further in the blend. Therefore a new density-dependent quenching mechanism must be invoked.

The TA kinetics in the GSB and PIA regions for the blend and neat films can be reconciled by introducing an ECA mechanism, as illustrated in Scheme 1. In this mechanism, photogenerated charges act as quenching sites for excitons in the vicinity. This leads to a kinetic competition in the blend between ECA, charge generation, and inherent exciton decay channels. The result of ECA is the return of an exciton to the ground state and optical excitation of a polaron state. The ECA model completely accounts for the observations presented in Figure 1 because i) the promptly generated population of charges evident from the ultrafast appearance of PIA can act as quenching sites for the remaining excitons (see Section 2.2 for quantification of RET rates); ii) exciton decay to the ground state is accelerated in the blend to produce a decaying GSB

signal over the timescale of excitons; and iii) diffusion-limited charge generation from excitons still occurs, albeit in competition with ECA, to produce a charge population that grows via the same kinetics as exciton decay in the blend and peaks at 100 ps. We will return to the P3HT/F8TBT system in later sections where the blend morphology dependence of TA kinetics and photocurrent extraction in a range of systems is shown to be consistent with the ECA model. In the next section, we will explore the RET mechanism for ECA in a range of organic semiconductor materials.

2.2. Resonant Energy Transfer Mechanism for Exciton-Charge Annihilation

The Förster theory can be applied to organic semiconductors to calculate the rate of RET between an emissive exciton (donor) and a resonantly absorbing polaron or charge pair (acceptor), with the RET radius R_0 given by:[25–27]

$$R_0^6 = \frac{9000(\ln 10)c^4\kappa^2}{128\pi^5\eta^4 N_{Av}} \int_0^\infty \frac{f_D(\nu)\varepsilon_A(\nu)}{\nu^4} d\nu \quad (1)$$

In Equation 1, R_0 is defined as the donor–acceptor distance where the rate of RET is equal to the radiative rate of the donor (rather than the sum of all decay rates). This modified form of the Förster equation avoids ambiguity when non-radiative decay rates are non-exponential and means that the emission quantum yield of the donor no longer appears in the expression for R_0.[6,27] The value of R_0 is strongly dependent on the spectral overlap integral between the emission spectrum of the donor $f_D(\nu)$ (in this case the P3HT fluorescence spectrum normalized such that $\int f_D(\nu)\, d\nu = 1$) and the absorption spectrum of the acceptor $\varepsilon_A(\nu)$ (in this case charges in P3HT and F8TBT) in units of molar extinction coefficient ($M^{-1}cm^{-1}$). Other variables and constants in Equation 1 are c (the speed of light), κ^2 (the orientation factor), η (the medium refractive index) and N_{Av} (Avagadro's number). The absorption spectrum of the acceptor is obtained in the appropriate units using:

$$\varepsilon(\nu) = \frac{\log_{10} e}{1000} N_{Av}\sigma(\nu) \quad (2)$$

where $\sigma(\nu)$ is the absorption cross-section of photogenerated charge pairs obtained from the transient transmission spectrum ($\Delta T/T(\nu)$) using:

$$\sigma(\nu) = -\frac{1}{Nz}\ln\left(1 + \frac{\Delta T}{T}(\nu)\right) \quad (3)$$

In Equation 3, z is the film thickness and the charge-pair density ($N = 2.3 \times 10^{18}$ cm^{-3}) is determined from the product of the incident fluence (10^{14} photons cm^{-2}), the absorption efficiency at the excitation wavelength ($\eta_{500\ nm} = 0.91$), the fraction of excitations that survive beyond 100 ps where the spectrum is measured ($\Phi = 0.20$, based on the relative remaining GSB intensity) divided by the film thickness ($z = 80$ nm). Finally, R_0 can be calculated after inserting N_{Av} (Avagadro's number) and estimates for the remaining variables in Equation 1. The orientation factor κ^2 is taken to be 0.655 for the case where the donor and acceptor dipoles are only constrained to lie in the plane of the film, although taking the isotropic value of $\kappa^2 = 2/3$ has a negligible impact,[6] and the refractive index η is estimated from published ellipsometry data to be ≈2.0 in this wavelength region.[28] We note that the quenching charge density (≈10^{18} cm^{-3}) exceeds the space-charge limit of charge density in a unipolar device (≈10^{17} cm^{-3}) and can only be achieved here because photogenerated charge pairs maintain overall charge neutrality in the film.

Figure 2a shows the overlap of donor (P3HT) emission and acceptor (P3HT/F8TBT charge pairs) absorption spectra.

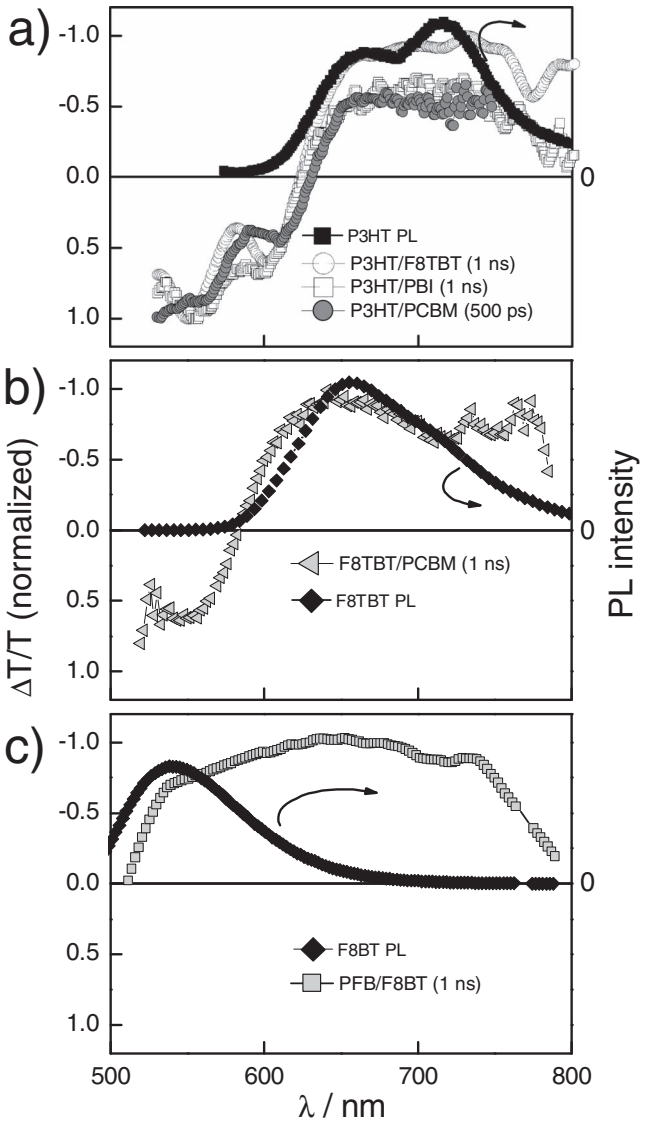

Figure 2. Resonance between charge-based PIA and excitonic PL for various donor acceptor blends: a) P3HT/F8TBT, P3HT/PBI, and P3HT/PCBM; b) F8TBT/PCBM; and c) PFB/F8BT. In all cases, TA spectra are obtained following 60 fs, 490–500 nm pulsed excitation with a fluence of ≈10^{14} photons cm^{-2} and sufficient pump–probe delay is used to ensure that charge generation is complete. The y -axes of TA spectra are inverted to highlight the resonance between PIA and steady state PL spectra.

Although excitation at 500 nm will also generate F8TBT-based excitons, RET will rapidly funnel these excitations to lower energy states in P3HT, hence its PL spectrum being taken as the donor. The strong spectral overlap in the 650–750 nm region for RET quenching by charges corresponds to $R_0 > 4.5$ nm.[29] At the excitation densities employed for the TA studies, the mean distance between initial excitations ($r = \sqrt[3]{(1/N_0)} = 4.4$ nm) is comparable to the calculated Förster radius, indicating that promptly photogenerated charge pairs in the P3HT/F8TBT blend are likely to quench nearby excitons at the fluences used. The extent of ECA expected will increase when considering effects beyond this simplistic assessment of mean donor-acceptor distances. Compounding effects include: i) excitons are mobile, thereby sampling a greater volume than that defined by the initial R_0 distance, and ii) an exciton can undergo multiple pairwise interactions with different quenching sites in a film, resulting in a cumulative quenching rate. We do not exclude the possibility of non-resonant energy transfer (i.e., the Dexter exchange mechanism), but we note that any process underpinned by electronic orbital overlap has an exponentially decaying rate with donor–acceptor distance, limiting its importance to the ≈1–2 nm range of electron tunneling in organic semiconductors. These compounding effects have been demonstrated in other systems with RET acceptors other than charges. In previous investigations of EEA in unblended fluorescent polymer films, exciton diffusion combined with RET radii of $R_0 \approx 4$ nm gives rise to critical exciton densities of $\approx 10^{18}$ cm^{-3} (i.e., 10 nm mean spacing between excitons).[6] The cumulative effect of exciton diffusion and long range RET are also found to considerably enhance apparent exciton diffusion lengths in multi-layered films with ground state RET acceptor layers.[30]

Comparison of RET overlap integrals also explains why ECA appears to be stronger than EEA in the donor-acceptor blend. The resonant EEA rate depends on the overlap of the exciton emission spectrum with the exciton absorption spectrum extracted from the TA spectrum. The TA spectrum of excitons in P3HT (Figure 1a) clearly lacks PIA in the 650–800 nm region of exciton emission. That is not to say that a PIA feature cannot exist in this region, but that it cannot couple strongly to a donor exciton because any PIA in that region is overwhelmed by SE with a stronger cross-section and opposite sign. As previously noted, the P3HT exciton PIA is centered at a much longer wavelengths than our spectral window and does not contribute appreciable overlap with the emission spectrum. Therefore we conclude that RET-based EEA is expected to be weaker than ECA in the P3HT/F8TBT blend.

The spectroscopic conditions that produced a large spectral overlap for ECA are by no means particular to this blend. On the contrary, resonance between excitons and charges in a given organic semiconductor should generally be expected owing to the common physical origins of both the exciton and polaron spectroscopic features, as illustrated in Scheme 1. As with π-conjugated molecules in solution, excitonic emission from organic semiconductor films is found to the red of the lowest energy absorption peak. The energy difference between absorption and emission bands (i.e., the Stokes shift) can largely be attributed to i) phonon energies being added to the vertical transition energy for absorption but subtracted for emission, ii) relaxation of the lattice (or solvent reorientation) around the excited state electronic configuration, and iii) exciton diffusion towards lower energy sites. It is no coincidence that polaron states are likely to absorb in the same spectral region as exciton emission. Polarons generally feature an absorption band on the red side of the main optical gap owing to the contracted π orbital splitting when the overall bond order is decreased (through oxidation or reduction of the neutral species).[31]

Figure 2a also shows the TA spectra of charge pairs in blends of P3HT with the electron acceptors [6,6]-phenyl-C_{61}-butyric acid methyl ester (PCBM) and perylene bisimide (PBI). The TA spectra were recorded under the same conditions as those in Figure 1a and are plotted with the emission spectrum of P3HT to highlight the resonance between exciton emission and charge absorption. In the case of the P3HT/PCBM blend, only holes in P3HT are visible in the TA spectrum owing to the absence of strong features from PCBM anions in this spectral region. Our previous investigations of charge photogeneration in the P3HT/PCBM blend also revealed an accelerated GSB signal that can be accounted for by considering ECA at the fluences used, as discussed further in Section 2.3.[16] In the case of the P3HT/PBI, like with P3HT/F8TBT, the PIA signal to the red of the optical gap includes contributions from both holes in P3HT and electrons in the acceptor phase. As we will describe in a future publication, ECA also complicates investigations of fast charge generation and recombination in donor-acceptor blends based on P3HT and perylene bisimide.[32]

Figure 2b,c illustrate comparably strong optical resonance between excitons and charges in donor–acceptor blends that do not include P3HT. The energy levels of F8TBT are suitably positioned for it to act as an electron donor when blended with a strong acceptor like PCBM. The TA spectrum in Figure 2b shows holes in F8TBT formed via photoexcitation of the blend (the PCBM-based electrons lack a significant absorption feature in this spectral region). The PIA feature in the 600–750 nm region is ideally positioned to act as a strong RET acceptor for emissive F8TBT excitons.

Figure 2c shows the TA spectrum of charge pairs in the blend of F8BT (poly(9,9′-dioctylfluorene-*alt*-benzothiadiazole) and PFB (poly(9,9-dioctylfluorene-*co*-bis-*N*,*N*′-(4,butylphenyl)-bis-*N*,*N*′-phenyl-1,4-phenylene-diamine), along with the PL spectrum of F8BT excitons. As previously reported, the spectral overlap between excitons and charges in the F8BT/PFB blend results in an R_0 of 4.24 nm, significantly higher than the R_0 calculated for EEA in F8BT (2.93 nm).[10] In that publication, evidence is reported for ECA in the F8BT/PFB blend based on similar observations that underpinned the ECA assignment in the P3HT/F8TBT blend discussed in Section 2.1. Given that relatively long-lived charges are generated rapidly and the GSB signal applies to both excitons and charges, the accelerated GSB decay observed in both blends can be explained by accelerated exciton decay to the ground state via annihilation with charges. In another investigation about longer lived excitations in the F8BT/PFB blend using TA spectroscopy on nanosecond to microsecond timescales, we found that ECA within the 600-ps excitation pulse accounted for the observed variation of the initial signal at ≈1 ns.[5]

Numerous recent reports have shown that charges can be photogenerated in a single material to some extent.[10,18,24,33] Even without heterojunction interfaces, charge photogeneration

can be induced from the energetic disorder present in different polymer microstructures (e.g., in P3HT),[24] by the strong donor–acceptor character of a given polymer[33] or by the presence of ions.[10] In the latter case, we have shown that charge-transfer states formed in the Coulomb field of ions have a PIA feature resonant with exciton emission, resulting in pronounced ECA under pulsed excitation. It is reasonable to assume that charge pairs formed in other neat polymer films could also lead to ECA. In the case of neat P3HT films, it is likely that the fluence dependence of exciton lifetimes is affected by both EEA and ECA reactions. Although the yield of direct charge photogeneration may be only 10% or less, the enhanced PIA of charges relative to excitons in the exciton emission spectral region means that the rate of RET is significantly greater between excitons and charges than between pairs of excitons. Therefore, even in films that exhibit a modest yield of direct charge photogeneration, ECA could still be operative at excitation densities below the threshold of EEA.

2.3. Effect of Blend Morphology on Exciton-Charge Annihilation

In bulk heterojunction blends there is a morphology dependent kinetic competition between excitons diffusing to charge generating interfaces and inherently decaying. At excitation densities sufficiently high for ECA but not for EEA and provided that charge recombination can be neglected on the exciton timescale, the simplest rate equations can be written as

$$\mathrm{Ex} \xrightarrow{k_0} \mathrm{GS} \tag{4}$$

$$\mathrm{Ex} \xrightarrow{k_{CT}} \mathrm{C} \tag{5}$$

$$\mathrm{Ex} + \mathrm{C} \xrightarrow{\gamma_{ECA}} \mathrm{GS} + \mathrm{C} \tag{6}$$

where excitons, charges, and ground states are represented by Ex, C, and GS, respectively, k_0 represents the inherent rate constant for exciton decay, k_{CT} the rate constant for charge generation, and γ_{ECA} the bimolecular rate constant for ECA.

The yield of charge generation can be easily calculated as a function of the different reaction channels that apply to excitons. The charge generation yield is given by

$$\Phi_{CT} = \frac{k_{CT}}{k_0 + k_{CT} + \gamma_{ECA}[C]} \tag{7}$$

And the ECA yield can be ascertained from the ratio of charge generation yields under conditions with and without ECA operating (the latter corresponding in practice to the low fluence limit)

$$\Phi_{ECA} = \frac{\gamma_{ECA}[C]}{k_0 + k_{CT} + \gamma_{ECA}[C]} = 1 - \frac{\Phi_{CT}(\mathrm{ECAon})}{\Phi_{CT}(\mathrm{ECAoff})} \tag{8}$$

We can consider the morphological dependence of each of the terms in the denominator of Equation 7 by examining the limiting and intermediate morphological/kinetic scenarios. **Figure 3** shows numerical simulations of the time-dependent evolution of charges and ECA rates along with the total yield of ECA for different morphologies, which are represented simplistically

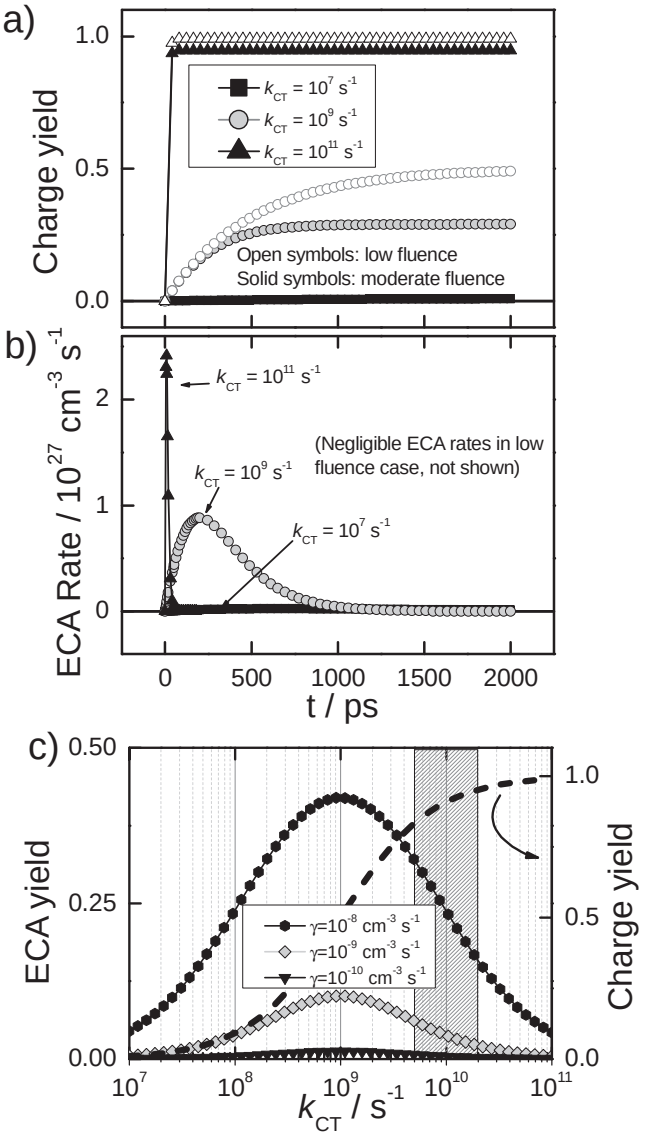

Figure 3. a) Numerical calculation of charge generation kinetics for various model morphologies. Charge transfer is modeled as a first order process competing with inherent exciton decay rate (k_0 = 10^9 s^{-1}) and exciton charge annihilation (γ_{ECA} = 10^{-8} cm^3 s^{-1}) from an initial exciton population of 10^{18} cm^{-3} (moderate fluence, solid symbols) and 10^{15} cm^{-3} (low fluence limit, open symbols). The charge transfer rate constants for each of the model blends are set to k_{CT} = 10^7 s^{-1} (coarse blend), k_{CT} = 10^9 s^{-1} (intermediate blend), and k_{CT} = 10^{11} s^{-1} (fine blend). Note that the fluence independent charge generation kinetics of the coarse blend obscures the low fluence symbols. b) Evolution of ECA rates for each of the model systems shown in part a with an initial exciton density of 10^{18} cm^{-3}. c) ECA yields (calculated as 1 – [Φ_{CT}(ECA on)/Φ_{CT}(ECA off)]) as a function of blend morphology (represented by k_{CT}) and γ_{ECA} for an excitation fluence of 10^{18} cm^{-3} following instantaneous excitation. Charge yields in the absence of ECA are also indicated, highlighting the optimal region for OPVs.

by the first order rate constant k_{CT}. For a strongly phase separated (coarse) blend or a bilayer with domains considerably larger than the exciton diffusion length, k_{CT} is much smaller than k_0 and even in the absence of ECA, a low charge generation yield results. Since ECA depends on the charge concentration, $\gamma_{ECA}[C] << k_0$ and will therefore only slightly reduce the already low charge generation yield. Most excitons will be formed too far away from an interface to undergo either charge transfer or ECA and there will be very little coexistence of excitons and charges, as shown in Figure 3a,b. For a very finely intermixed blend, on the other hand, Equation 7 predicts that the charge generation yield will be unaffected by ECA but for a different reason. Here, k_{CT} is the dominant channel since all excitons are generated sufficiently close to heterojunctions for rapid charge transfer. This kinetic scenario means that the period of coexisting exciton and charge populations (i.e., appreciable ECA rate) is constrained to a timescale that is too short for ECA to have much effect and the yield of charge photogeneration remains high, as shown in Figure 3a,b. These limiting cases suggest that ECA will have the largest impact in the intermediate kinetic/morphological regime, where k_{CT} is high enough to produce a large population of charges, but low enough to also leave a large population of excitons vulnerable to interactions with charges for a relatively long time. Figure 3c demonstrates that ECA is infact strongest where $k_0 = k_{CT}$, i.e., where there would be a 50% yield of charges formed in the absence of ECA.

Importantly from the perspective of probing charge photogeneration in OPVs, the most effective morphology for photocurrent generation is vulnerable to significant ECA. This is particularly true of polymer/polymer blend OPVs. A moderately phase separated morphology optimizes the conflicting morphological requirements of exciton quenching (favoring small phases) and complete dissociation and extraction of interfacial charge pairs (favoring large phases).[22] In other words, the optimum bulk heterojunction OPV morphology for many materials has phases that are only just small enough for most excitons to eventually reach a charge generation interface. An ideal polymer/polymer blend morphology prolongs exciton lifetimes while maintaining a high charge generation yield, therefore coexisting populations of excitons and charges are maximized under pulsed excitation. It is worth noting that the phase behavior of polymer–fullerene blends can be more complicated. For example, fullerene molecules have been found to form highly ordered intercalated structures with polymers such as pBTTT (poly(2,5-bis(3-tetradecylthiophen-2-yl)thieno[3,2-b] thiophene) whose sidechain spacings are matched to the free volume requirements of the fullerene.[34] In these phases, excitons are completely quenched by the infiltrated fullerene without the need for exciton diffusion. The extremely high value of k_{CT} in these phases would preclude ECA, but the high ordering still permits sufficiently high and balanced charge mobilities that reasonable photovoltaic efficiencies are observed.[34]

The sidechains in P3HT are too closely spaced for infiltration of PCBM,[34] and the exclusion of PCBM from P3HT phases upon thermal annealing is linked to improved photocurrent yields.[16,17] **Figure 4**a demonstrates the emergence of ECA in a P3HT/PCBM blend whose morphology is optimized for photocurrent generation via thermal annealing. In the pristine

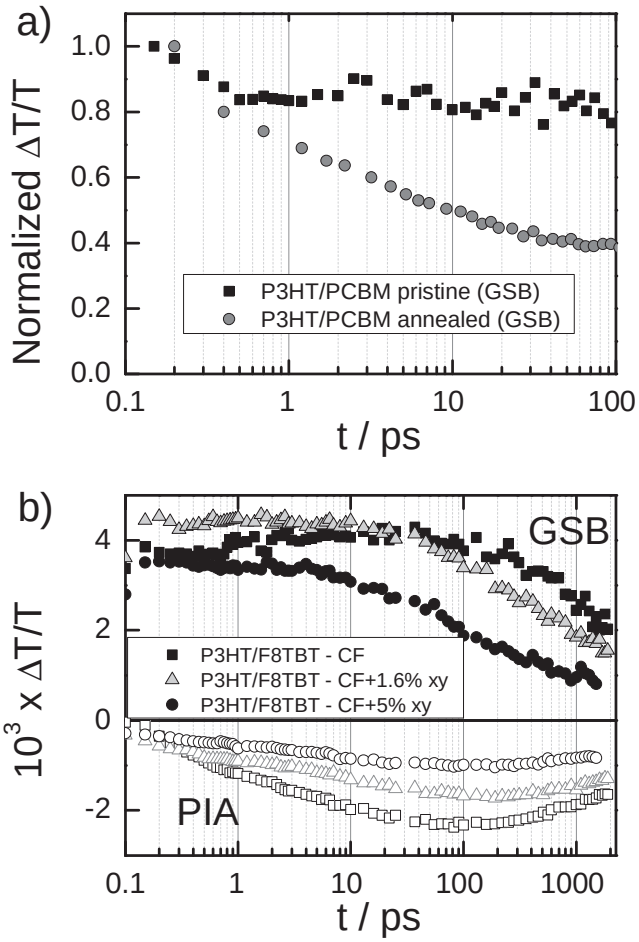

Figure 4. Morphology dependence of ECA probed via GSB recovery kinetics for donor-acceptor blends of different morphologies following 60 fs, 500 nm pulsed excitation with fluences of $\approx 10^{14}$ photons cm^{-2}. a) Pristine versus thermally annealed blends of P3HT/PCBM cast from chloroform probed in the P3HT GSB region of 530–570 nm. b) Blends of P3HT/F8TBT cast from mixtures of chloroform (CF) and varying amounts of the higher boiling point solvent xylene (xy) to induce coarser film formation.[22] Kinetics are shown for both the GSB region (530–570 nm, solid symbols) and the charge-based PIA region (650–700 nm, open symbols with shapes corresponding to legend).

blend, ultrafast and quantitative charge photogeneration is evident from the arrested decay of the GSB signal that applies to both excitons and charges and the corresponding ultrafast appearance of a charge-based PIA signal, as we have previously described.[16] However, the external quantum efficiency of the device (peaked at 30%) suffers from inefficient extraction of the charges. The quantum efficiency nearly doubles to over 50% upon thermal annealing to achieve a morphology that balances the requirements of charge generation and extraction. When the thermally annealed blend is measured under the same excitation conditions, charge generation kinetics probed via the PIA growth are slowed to a timescale of ≈4 ps. The observed rate of charge transfer is still sufficiently high that near unit charge yield would be expected, in which case one would expect the GSB signal from excitons to be retained with the formation of

charges. However, Figure 4a shows that the GSB signal decays by ≈50% within the first 10 ps. One possible explanation for the observed GSB decay is that charges could be undergoing dynamic localization (self-trapping) on this timescale, thereby bleaching a smaller chromophore volume and producing a corresponding reduction on the GSB intensity over time. However, we also observe a ≈50% reduction in the external quantum efficiency of the device under the same pulsed excitation conditions compared with weak steady state illumination, suggesting that accelerated population decay under pulsed excitation must be considered to be the more likely explanation for the GSB decay. Since the GSB decays with the same kinetics as charge generation, we can conclude that the accelerated population decay applies to excitons (i.e., from ECA) rather than charges (i.e., from bimolecular charge recombination).

We have previously shown that the degree of phase separation in polymer/polymer blends including P3HT/F8TBT can be tuned by adjusting the composition of the solvent from which the blend is cast. Spin coating from a volatile solvent like chloroform results in a finely intermixed blend, whereas adding up to 5% of a less volatile solvent such as xylene produces a much coarser morphology and a more efficient OPV device. Figure 4b shows the GSB and PIA kinetics for three different P3HT/F8TBT blends whose morphologies were tuned via the cosolvent method. In all cases, charge recombination depletes the PIA and GSB signals beyond 100 ps. The three blends exhibit substantially different behavior for the first 100 ps owing to the morphological dependence of charge transfer rates. The kinetics for the blend cast from chloroform with 5% xylene are very similar to the thermally annealed blend described in Section 2.1; substantial decay of the GSB within the first 100 ps is strong evidence of ECA competing with charge transfer. In the finely mixed blend cast from neat chloroform, however, the GSB signal remains approximately constant until the onset of charge recombination beyond 100 ps. Since the GSB signal reflects the total population of excitons and charges, its maintenance over the first 100 ps shows that charge transfer has unit efficiency and ECA does not compete effectively in a finely mixed blend. The growth of the PIA signal therefore reflects diffusion of excitons to charge generating interfaces without the interference of ECA. As expected, the GSB kinetics of the blend cast from chloroform with 1.6% xylene fit in between those of fine and coarse blends. It may seem contradictory that all three blends appear to have the same charge generation kinetics (based on PIA) in spite of quite different morphologies. These observations can be reconciled when ECA is taken into account. The charge generation kinetics observed via the PIA signal depend on the exciton lifetime, which in turn depends on the sum of all rate constants which deplete the exciton, i.e., $\tau_{Ex} = 1/(k_0 + k_{CT} + \gamma_{ECA}[C])$. In the coarsest blend, the longer average distance required for an exciton to reach a heterojunction reduces k_{CT}, but this is offset by long-range ECA becoming important in the coarser blend. If the reduction in k_{CT} is balanced by an increase in $\gamma_{ECA}[C]$, the normalized PIA kinetics will be independent of morphology and the peak charge yield will diminish according to Equation 7. The numerical simulations in Figure 3a also illustrate this point; in the absence of ECA, charge populations approach their maximal values at later times when k_{CT} is decreased (representative of morphology coarsening). This trend is diminished when ECA operates because charge growth kinetics, are accelerated, albeit with lower charge yields. The PIA kinetic measurements in Figure 4b show that this is indeed the case; all three blends have a charge population peaked at 100 ps, while the charge yield in the coarsest blend is approximately half that of the finest blend owing to competition with ECA within the first 100 ps and consistent with the loss of approximately half of the GSB signal within the first 100 ps. The stronger effect of ECA in coarser blends implies that the observed charge generation kinetics in these blends are biased towards those excitons created sufficiently close to an interface for charge generation to outcompete ECA. This gives rise to an apparent morphological independence that is actually an artifact of high intensity pulsed excitation. If it were not for ECA, peak charge populations would be expected to occur later for coarser blends and charge yields would only be reduced when charge generation became too slow to compete with the inherent monomolecular decay of excitons (k_0).

2.4. Fluence Dependence of Exciton-Charge Annihilation

ECA is a bimolecular process that would not be observed in the limit of low excitation fluence. The rate of ECA will increase according to $\gamma_{ECA}[Ex][C]$, which leads to a quadratic dependence on excitation intensity since without ECA, both [Ex] and [C] are linearly dependent on intensity (in addition to their morphology dependence, as discussed in Section 2.3). We note that the Förster RET model also predicts a quadratic intensity dependence. The average donor–acceptor distance (r_{av}) can be related to the excitation density (N) by $r_{av} = (1/N)^{1/3}$, which is propotional to $(1/I)^{1/3}$ since N is propotional to the intensity (I). A quadratic intensity dependence for the RET rate is revealed when this expression for r_{av} is substituted into the rate expression for RET ($k_{RET} \approx 1/r^6$). Our previous measurements of charge photogeneration in P3HT/PCBM blends demonstrate that the total population of excitations that survive beyond the exciton timescale (probed via GSB intensity) is indeed strongly dependent on intensity and blend morphology.[16] Signal sensitivity limits the range of intensities over which ECA can be easily quantified using optical probes. Even the lowest measureable excitation fluences are often slightly above the threshold for ECA. A straightforward alternative method for observing the effect of bimolecular processes under a wider range of pulsed excitation intensities is to measure the extracted photocurrent. As is the case with other bimolecular processes that limit photocurrent extraction (e.g., bimolecular charge recombination), the operation of ECA is identified by a square-root dependence of photocurrent on excitation intensity.

Figure 5 shows the photocurrent collected from pairs of P3HT/F8TBT and P3HT/PCBM devices over two orders of magnitude in pulsed excitation intensity. The pairs of devices have the same active layer composition cast from chloroform and one of each pair of devices is subsequently thermally annealed to produce a coarser blend morphology. In the case of the annealed P3HT/F8TBT device, the intensity dependent photocurrent is well fit by a line proportional to $I^{0.53}$ over this intensity range, consistent with the square root intensity dependence expected for second order loss mechanisms. The external quantum efficiency at the

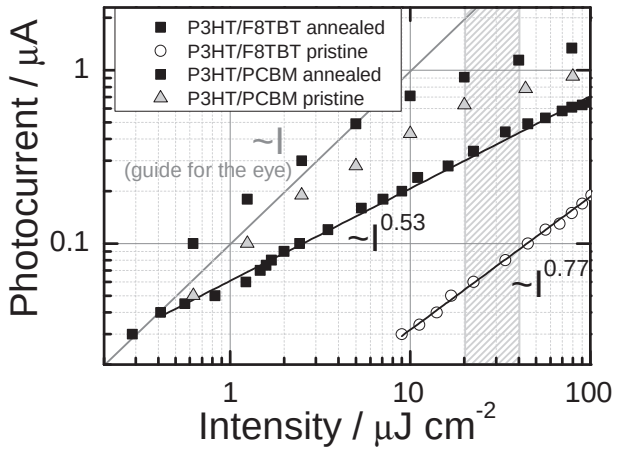

Figure 5. Fluence-dependent short circuit photocurrent for a pristine and a thermally annealed P3HT/F8TBT and P3HT/PCBM devices following 500 nm pulsed excitation with 100 fs and 60 fs pulsewidths, respectively. The expected linear dependence of photocurrent in the absence of bimolecular losses is shown as a guide for the eye. Linear fits of observed data are also shown for the P3HT/F8TBT devices to highlight the greater degree of bimolecular losses suffered in the annealed blend than in the pristine blend. The shaded region represents the approximate fluences where TA kinetics were optically measured in other sections of this paper.

lowest pulsed intensity (28%) approaches the steady state value, suggesting that the sublinear threshold is around 0.4 μJ cm^{-2} in this device. Undoubtedly, other second order processes in addition to ECA can play a role at the intensities shown. However, the optical TA measurements shown in Figure 1b and 4b clearly show that ECA must strongly contribute to the sublinear behavior at the intensity where TA measurements were carried out (also indicated on Figure 5). In contrast, the photocurrent extracted from the pristine P3HT/F8TBT device is proportional to $I^{0.77}$ over the measured intensity range. The weaker suppression of photocurrent is consistent with the TA measurements shown in Figure 4, which demonstrated that ECA is less pronounced in a fine blend morphology (i.e., the pristine blend cast from chloroform).

The intensity dependent photocurrent measurement for the annealed P3HT/PCBM blend device exhibits a transition from a nearly linear photocurrent regime to a sublinear regime ($\approx I^{-0.5}$) in the vicinity of ≈7 μJ cm^{-2}. This fluence corresponds to an initial excitation density of approximately 10^{18} cm^{-3} and a mean distance between initial excitations of 10 nm. We highlight the fact that the threshold lengthscale corresponds closely to the size of pure crystalline P3HT aggregates formed via thermal annealing. Again, TA spectroscopy confirms that ECA is a significant source of the sublinearity in this fluence regime for the annealed blend (see Figure 4a), as expected if mobile excitons can interact with multiple charges and the pairwise RET radius for ECA is ≈4 nm.

2.4. Implications for Time-Resolved Spectroscopy of Charge Photogeneration

TA spectroscopy on femtosecond to nanosecond timescales with a ≈1 kHz pulse repetition rate typically requires an excitation fluence of over 10^{13} photons cm^{-2} in order to produce sufficiently strong differential transmission signals ($|\Delta T/T| > 10^{-4}$) to reliably resolve the dynamics of intermediates. These figures already represent considerable recent advances in signal sensitivity from noise suppression strategies such as multichannel shot-to-shot detection and shot discrimination.[10] For typical organic semiconductor films that are ≈100 nm thick and have an optical density of ≈0.5 at the excitation wavelength, this minimum resolvable fluence corresponds to an initial excitation density of ≈7 × 10^{17} cm^{-3}. EEA can usually be avoided with excitation fluences on this order, as evident by entering a fluence-independent regime in measurements of nonblended polymers.[18,20] However excitation fluences for blended films capable of ECA cannot be set on the basis of the absence of EEA in nonblended films because ECA can be a stronger effect. Determining the linear photocurrent regime under pulsed excitation may often be a more appropriate and simpler way of determining an excitation density where ECA can be excluded prior to making TA measurements. The linear dependence of photocurrent upon intensity for the P3HT/PCBM devices shown in Figure 5 suggests that the effects of ECA could be avoided if TA could be undertaken at fluences as low as ≈5 μJ cm^{-2}. Even lower fluences would be required in order to exclude the possibility of ECA in the P3HT/F8TBT devices, unless all observed bimolecular losses at ≈5 μJ cm^{-2} can be attributed to other effects such as bimolecular charge recombination. In general, the excitation density threshold of ECA for various blend morphologies is in the vicinity of the minimal measureable TA signals and ECA is therefore an artifact worth considering in any TA measurement of charge photogeneration.

Higher signal sensitivity can often be achieved using lasers with higher pulse repetition rates (and lower pulse energies).[7] Reducing pulse energies is an effective way of avoiding EEA, however it is worth noting that ECA is not as easily avoided by increased repetition rates due to the longer lifetime of charges. For example, increasing the laser repetition rate from 1 kHz to 100 kHz would be expected to yield an order of magnitude ($n^{1/2}$) improvement in signal sensitivity and therefore permit measurements with ten times lower pulse energies. However, the reduced period between pulses (10 μs compared with 1 ms) will likely overlap with the charge lifetime, therefore a steady state population of charges will remain as quenching sites when each new excitation pulse produces excitons. In this example, the steady state charge population would be over half of the peak charge population if charges decayed exponentially with a lifetime of 10 μs.[35] The steady state charge population could have a greater effect on ECA than the new charge population generated from a given pulse because the steady state charge population already exists at the time of maximal exciton population (i.e., immediately after each excitation pulse). The order of magnitude improvement in signal sensitivity achieved by higher repetition rate excitation would be offset to a significant degree by the increase in ECA rate caused by the steady state charge population.

While this article has focused on ECA over ps-ns timescales following ≈100 fs excitation where exciton quenching can be directly resolved, ECA can also influence TA measurements on longer timescales. TA spectroscopy on nanosecond to millisecond timescales is frequently used to assess charge photogeneration yields and recombination rates.[1,2,17] The longer pulsewidth of excitation pulses in those experiments (≈600 ps–7 ns),

precludes resolution of exciton dynamics, but the impact of ECA is comparable for a given pulse energy. Nanosecond excitation pulses are likely to be longer than the charge generation timescale but shorter than that of recombination. This kinetic scenario retains strong temporal overlap of excitons and charges within the excitation pulse because charges that accumulate throughout the pulse are available to interact with subsequently generated excitons. The numerical calculations of ECA yields in Figure 3c appear almost identical if a 5 ns Gaussian excitation profile is used instead of an infinitely short excitation pulse of the same fluence (data not shown). Our previous investigations of the nanosecond to microsecond dynamics in F8BT/PFB blends demonstrated that the yield of excitations is indeed subject to ECA within the excitation pulse, which accounted for the sublinear intensity dependence of the initial nanosecond signal intensity.[5]

TA spectroscopy on microsecond timescales is frequently used as a simple optical assay of charge population.[20] Such experiments are typically carried out with low repetition rate excitation (≈4–10 Hz) and excitation densities on the order of 10^{18} cm^{-3}. This creates the strong possibility of ECA within the excitation pulse, which will lead to underestimation of the charge population. This might be an acceptable artifact if its effect was constant across the series of samples to be compared. However, as this article highlights, the magnitude of ECA has a strong morphological dependence. For microsecond TA measurements of films with different morphologies, using excitation fluences high enough for ECA will introduce a bias that systematically decreases the measured charge yields for coarser morphologies. Moreover, if charge recombination mechanisms are the focus of microsecond TA measurements, one must be aware that operation of ECA will bias the observed population of charges towards those generated in smaller domains, which will potentially exhibit only a subset of recombination mechanisms (e.g., a greater likelihood of bound charge-transfer states).

The sensitivity limits of transient optical experiments may often mean that ECA is practically unavoidable. It therefore becomes imperative to recognize its effects. For TA measurements on timescales where excitons still exist, accelerated GSB decay is often a clear signature of ECA. The magnitude of GSB decay can be used to quantify the efficiency of the ECA branch under given excitation conditions and thereby renormalize the dynamics of other processes as an approximation of low-intensity regime kinetics. For TA measurements with longer excitation pulses, operation of ECA will result in a sublinear dependence of initial optical signatures on excitation intensity and a morphological bias to the surviving charge population.

3. Conclusions

Our TA spectroscopy measurements highlight the significance of ECA reactions in blended organic semiconductor films at excitation densities of ≈10^{18} cm^{-3}. This scenario could be encountered as a strong loss mechanism in devices (including organic lasers and OPVs for concentrated solar applications). In spite of their short lifetimes, singlet excitons are strongly quenched by charges due to strong optical resonance for RET, which we show is a general feature in organic semiconductors owing to the stabilization energies of excitons and polarons. We explore the morphology dependence of ECA in donor–acceptor blends where the timescale of coexisting excitons and charges varies. We find that this leads to a pronounced morphology dependence of ECA, with the greatest impact in systems with moderate charge transfer rates, i.e., well-balanced with the inherent rate of exciton decay.

As we highlight in this article, ECA is an extremely important consideration in TA measurements of charge generation in OPV films under pulsed excitation. This results from the practical need to use excitation densities on the order of the ECA threshold, along with optimal OPV blend morphologies that often enhance the coexistence of excitons and charges. ECA is clearly identified in TA measurements by simultaneously probing optical signatures of excitons, charges, and the total population of excitations throughout the timescale of excitons in different materials and blend morphologies. One important consequence of ECA is that it masks the morphological dependence of charge generation kinetics. We also see evidence of ECA in intensity-dependent measurements of photocurrent over a wide range of pulsed excitation densities in OPV devices. As well as highlighting the value of TA spectroscopy in interrogating ECA, this article shows that accounting for the effects of ECA is essential in order to uncover intrinsic charge generation in TA spectroscopy measurements of OPV blends.

4. Experimental Section

Sample Preparation: Samples for spectroscopy were spin-coated onto spectrosil quartz substrates that were previously cleaned via sonicating successively in acetone and isopropyl alcohol. Film thicknesses were typically between 80 and 120 nm (with pertinent details about film thicknesses and casting solvents noted throughout the text where necessary). Where required, films were annealed on a hotplate at 140 °C in an inert atmosphere for 10 min immediately after spin-coating. Further details about thin film preparation and the fabrication and characterization of devices can be found in previous publications relating blends of P3HT/F8TBT,[11,22] PFB/F8BT,[10,22] F8TBT/PCBM,[36] and P3HT/PCBM.[16]

Spectroscopy: UV-visible absorption spectra were measured with a Hewlett Packard 8453 UV-visible system. Steady-state room-temperature PL measurements on thin films were undertaken using a Varian Cary Eclipse Fluorescence spectrometer.

Samples for TA spectroscopy were kept under dynamic vacuum (≈10^{-5} mbar). TA spectroscopy was carried out using previously described methods.[10] Pulsed excitation was provided by 60-fs output of a TOPAS (Light Conversion Ltd.), with excitation wavelengths and fluences noted for each blend. Broadband probe pulses were generated in a non-collinear optical parametric amplifier. Special care was taken to ensure that the spatial overlap of excitation and probe beams was maintained throughout the entire range of delay stage translation. In fluence-dependent photocurrent measurements, the photocurrent from encapsulated devices was measured using a Keithley source-measure unit upon illuminated with the same pulsed laser excitation source as for TA spectroscopy.

Numerical Calculations: The numerical calculations of charge transfer dynamics under the influence of ECA were carried out by solving the rate Equations 4–6 in the MATLAB software package and applying Equations 7 and 8 to obtain charge transfer and ECA yields.

Acknowledgements

The authors acknowledge the U.K. Engineering and Physical Sciences Research Council (EPSRC) for funding.

Received: October 10, 2011
Revised: December 23, 2011
Published online: February 16, 2012

[1] C. G. Shuttle, R. Hamilton, B. C. O'Regan, J. Nelson, J. R. Durrant, *Proc. Nat. Acad. Sci. USA* **2010**, *107*, 16448.
[2] F. Etzold, I. A. Howard, R. Mauer, M. Meister, T.-D. Kim, K.-S. Lee, N. S. Baek, F. Laquai, *J. Am. Chem. Soc.* **2011**, *133*, 9469.
[3] T. N. Singh-Rachford, F. N. Castellano, *Coord. Chem. Rev.* **2010**, *254*, 2560.
[4] D. Hertel, K. Meerholz, *J. Phys. Chem. B* **2007**, *111*, 12075.
[5] I. A. Howard, J. M. Hodgkiss, X. Zhang, K. R. Kirov, H. A. Bronstein, C. K. Williams, R. H. Friend, S. Westenhoff, N. C. Greenham, *J. Am. Chem. Soc.* **2010**, *132*, 328.
[6] M. A. Stevens, C. Silva, D. M. Russell, R. H. Friend, *Phys. Rev. B* **2001**, *63*, 165213.
[7] S. M. King, D. Dai, C. Rothe, A. P. Monkman, *Phys. Rev. B* **2007**, *76*, 085204.
[8] M. A. Baldo, R. J. Holmes, S. R. Forrest, *Phys. Rev. B* **2002**, *66*, 035321.
[9] A. J. Ferguson, N. Kopidakis, S. E. Shaheen, G. Rumbles, *J. Phys. Chem. C* **2008**, *112*, 9865.
[10] J. M. Hodgkiss, G. Tu, S. Albert-Seifried, W. T. S. Huck, R. H. Friend, *J. Am. Chem. Soc.* **2009**, *131*, 8913.
[11] J. M. Hodgkiss, A. R. Campbell, R. A. Marsh, A. Rao, S. Albert-Seifried, R. H. Friend, *Phys. Rev. Lett.* **2010**, *104*, 177701.
[12] J. Zaumseil, R. H. Friend, H. Sirringhaus, *Nat. Mater.* **2006**, *5*, 69.
[13] T. Drori, C.-X. Sheng, A. Ndobe, S. Singh, J. Holt, Z. V. Vardeny, *Phys. Rev. Lett.* **2008**, *101*, 037401.
[14] T. Offermans, S. J. C. Meskers, R. A. J. Janssen, *Chem. Phys.* **2003**, *119*, 10924.
[15] S. C. J. Meskers, P. A. van Hal, A. J. H. Spiering, J. C. Hummelen, A. F. G. van de Meer, R. A. J. Janssen, *Phys. Rev. B* **2000**, *61*, 9917.
[16] R. A. Marsh, J. M. Hodgkiss, S. Albert-Seifried, R. H. Friend, *Nano Lett.* **2010**, *10*, 923.
[17] R. A. Marsh, J. M. Hodgkiss, R. H. Friend, *Adv. Mater.* **2010**, *22*, 3672.
[18] S. De, T. Pascher, M. Maiti, K. G. Jespersen, T. Kesti, F. Zhang, Ö. Inganas, A. Yartsev, V. Sundstrom, *J. Am. Chem. Soc.* **2007**, *129*, 8466.
[19] J. Piris, T. E. Dykstra, A. A. Bakulin, P. H. M. van Loosdrecht, W. Knulst, M. T. Trinh, J. M. Schins, L. D.A. Siebbeles, *J. Phys. Chem. C* **2009**, *113*, 14500.
[20] H. Ohkita, S. Cook, Y. Astuti, W. Duffy, S. Tierney, W. Zhang, M. Heeney, I. McCulloch, J. Nelson, D. D. C. Bradley, J. R. Durrant, *J. Am. Chem. Soc.* **2008**, *130*, 3030.
[21] J. Guo, H. Ohkita, H. Benten, S. Ito, *J. Am. Chem. Soc.* **2010**, *132*, 6154.
[22] A. R. Campbell, J. M. Hodgkiss, S. Westenhoff, I. A. Howard, R. A. Marsh, C. R. McNeill, R. H. Friend, N. C. Greenham, *Nano Lett.* **2008**, *8*, 3942.
[23] S. Albert-Seifried, R. H. Friend, *Appl. Phys. Lett.* **2011**, *98*, 223304.
[24] F. Paquin, G. Latini, M. Sakowicz, P.-L. Karsenti, L. Wang, D. Beljonne, N. Stingelin, C. Silva, *Phys. Rev. Lett.* **2011**, *106*, 197401.
[25] T. Förster, *Ann. Phys. (Leipzig)* **1948**, *2*, 55.
[26] T. Förster, *Discuss. Faraday Soc.* **1959**, *27*, 7.
[27] L. N. M. Duysens, *Prog. Biophys. Mol. Biol.* **1964**, *14*, 1.
[28] M. Campoy-Quiles, J. Nelson, D. D. C. Bradley, P. G. Etchegoin, *Phys. Rev. B* **2007**, *76*, 235206.
[29] This is a lower limit estimation of R_0 since the TA spectrum is truncated where probe pulses become too weak beyond 730 nm.
[30] W. A. Luhman, R. J. Holmes, *Adv. Funct. Mater.* **2011**, *21*, 764.
[31] P. J. Brown, H. Sirringhaus, M. Harrison, M. Shkunov, R. H. Friend, *Phys. Rev. B* **2001**, *63*, 125204.
[32] S. Hüttner, J. M. Hodgkiss, M. Sommer, R. H. Friend, U. Steiner, M. Thelakkat, *unpublished*.
[33] M. Westerling, H. Aarnio, R. Österbacka, H. Stubb, S. M. King, A. P. Monkman, M. R. Andersson, K. Jespersen, T. Kesti, A. Yartsev, V. Sundström, *Phys. Rev. B* **2007**, *75*, 224306.
[34] A. C. Mayer, M. F. Toney, S. R. Scully, J. Rivnay, C. J. Brabec, M. Scharber, M. Koppe, M. Heeney, I. McCulloch, M. D. McGehee, *Adv. Funct. Mater.* **2009**, *19*, 1173.
[35] If the time between pulses is equal to the charge lifetime (assumed for simplicity to be exponential), then the proportion of charges that remain from the previous pulse is 1/e. Adding the residuals from all previous pulses gives the geometric series $(1/e) + (1/e)^2 + (1/e)^3 + \ldots$, which sums to $1/(1-(1/e)) - 1 = 0.58$.
[36] C. R. McNeill, A. Abrusci, J. Zaumseil1, R. Wilson, M. J. McKiernan, J. H. Burroughes, J. J. M. Halls, N. C. Greenham, R. H. Friend, *Appl. Phys. Lett.* **2007**, *90*, 193506.